Journal of Applied Biology & Biotechnology Vol. 12(2), pp. 304-311, Mar-Apr, 2024
Available online at http://www.jabonline.in
DOI: 10.7324/JABB.2024.176603

In silico analysis of garlic phytochemicals binding affinities to skeletal muscle atrophy linked factors through molecular docking

Monika Monika[1]*, Sanjeev Gupta[1], Anita Dua[2], Ashwani Mittal[2]

[1]Department of Zoology, IIHS, Kurukshetra University, Kurukshetra, Haryana, India.
[2]Cell Biology Lab, Department of Biochemistry, IIHS, Kurukshetra University, Kurukshetra, Haryana, India.

ARTICLE INFO

Article history:
Received on: November 07, 2023
Accepted on: January 02, 2024
Available online: Febuary 20, 2024

Key words:
Molecular docking,
Ligand receptor interactions,
Skeletal muscle atrophy,
Austalide A,
Natural compounds.

ABSTRACT

Skeletal muscle atrophy, which involves the loss of skeletal muscle function, can be triggered by pathological factors such as disuse, cancer cachexia, and aging. This condition is characterized by decreased muscle fiber size, reduced myonuclear count, and subsequent weakening of muscle strength accompanied by depletion of contractile proteins. Imbalances in anabolic hormones, elevated levels of transforming growth factor β, myostatin, cytokines (such as tumor necrosis factor-alpha, TWEAK, and interleukin-6), oxidative stress, and limited availability of amino acids further contribute to the progression of muscle atrophy. To date, there are no FDA-approved drugs available for skeletal muscle atrophy. In this study, we conducted molecular docking using HR-LCMS-QTOF identified garlic compounds (375) against key targets involved in skeletal muscle atrophy, including histone deacetylase 4, Nuclear factor kappa-light-chain-enhancer of activated B cells, Atrogin, Murf1, mammalian target of the rapamycin, Myostatin, insulin like growth factor-1, and Beclin. These targets play crucial roles in the mechanism of skeletal muscle atrophy. Among the 375 compounds analyzed, austalide A exhibited the highest binding affinity with all targets. The current study findings provide a base for continued exploration of these natural compounds in the development of skeletal muscle atrophy therapeutics.

1. INTRODUCTION

Skeletal muscle is an essential tissue that constitutes approximately 40% of the body weight and encompasses around 50% of the total protein content. The somatic nervous system regulates skeletal muscles, enabling control over body posture, facilitating gestures, and supporting locomotion [1]. The fundamental functional units of skeletal muscles are sarcomeres, which consist of two types of filaments: actin (thin filaments) and myosin (thick filaments) [2]. Skeletal muscles are classified into three types based on their myosin-heavy chain composition: Type-I (characterized by slow contraction and high mitochondrial content), Type-IIa (exhibiting fast contraction and reliance on oxidative phosphorylation), and Type-IIb (also fast-contracting but with reduced ATP production).

Skeletal muscle function relies on a well-coordinated balance between protein synthesis and degradation, maintaining its integrity [3,4]. Protein metabolism changes in response to various external stimuli or biological factors. Muscle atrophy occurs in three different forms: Primary atrophy (caused by inherited myopathies), secondary skeletal muscle atrophy (arising from underlying diseased conditions), or age-related atrophy (known as sarcopenia) [5]. Secondary muscle atrophy is influenced by diverse factors, including diseases such as cancer, AIDS, diabetes, chronic diseases, and long-term infections, as well as aging, starvation, and physical inactivity. Skeletal muscle atrophy is characterized by specific alterations in muscle structure, including the shrinkage of myofibers, changes in the composition of myosin isoforms (types of muscle proteins), loss of cytoplasm, organelles, and overall protein content [6].

Muscle atrophy is a complex process with mechanisms that are not fully understood [Figure 1]. Increased oxidative stress, inflammation, and impaired mitochondrial functions caused by various diseases are important early signals in skeletal muscle atrophy [7]. Protein degradation in muscle atrophy involves multiple systems: The ubiquitin-proteasome system, autophagy-lysosome system, caspase, and calpain systems that are involved in proteolytic processing, modifying substrate structures and activities [8-10]. These degradation systems do not work independently but rather interact in a complex manner and result in complete protein degradation [11-13]. Skeletal muscle, alongside other cells, secretes IL-6, which activates STAT3 protein and promotes skeletal muscle protein degradation by inhibiting JAK/STAT3, ERK, and PI3K/Akt signaling pathways [14]. Additionally, TNF-α, a multifunctional cytokine, inhibits protein synthesis and accelerates protein degradation, particularly implicated in skeletal muscle protein loss

*Corresponding Author:
Monika Monika,
Department of Zoology, IIHS, Kurukshetra University,
Kurukshetra, Haryana, India.
E-mail: monikay167 @ kuk.ac.in

associated with aging, cancer, and chronic obstructive pulmonary disease [15,16].

MuRF1 and Atrogin-1 are crucial ubiquitin ligases involved in muscle atrophy. MuRF1 targets myofibrillar proteins, while Atrogin-1 ubiquitinates desmin and vimentin, both associated with the sarcomere structure. Inhibiting these ligases shows potential for treating muscle atrophy [17-21]. Autophagy (the degradation process of cytoplasmic contents and organelles in lysosomes), is normally low in skeletal muscles, but it is significantly upregulated in pathological conditions such as oxidative stress, denervation, and fasting, leading to protein degradation. FOXO3, a transcriptional regulator, controls key autophagy genes, including Bnip3, Gabarap, LC3, and Atg12 in muscle. The p38/MAPK pathway and downregulated histone deacetylases (HDAC) also influence autophagy levels under oxidative stress [22-26]. Caspases are protease enzymes that cleave various substrates, including actomyosin complexes, contributing to skeletal muscle wasting. Caspase-3 plays a key role by stimulating UPS-mediated protein degradation. There is crosstalk between calpain and caspase-3, where calpain promotes caspase-3 activation and vice versa [27-30]. Calpains, calcium-dependent cysteine proteases, including calpain 1 (μ-calpain) and calpain 2 (m-calpain), contribute to myofibril degradation. Molecular events such as SMYD2 glutathionylation, GSK3-β phosphorylation of desmin filaments, and CaMKIIβ signaling regulate calpain activity [31-35].

The mammalian target of the rapamycin (mTOR) pathway, consisting of mTOR complex 1(mTORC1), and mTOR complex 2 (mTORC2), plays a crucial role in regulating protein translation, autophagy, ribosome biogenesis, and cell proliferation [36-38]. The transforming growth factor β family, including myostatin, regulates skeletal muscle regeneration and fibrosis. Myostatin, through activation of Smad2/3 and protein ubiquitination degradation, negatively affects muscle mass, while inhibiting Smad2/3 alone is sufficient to induce muscle growth [39,40]. HDAC4 plays a role in skeletal muscle atrophy by repressing muscle-specific gene expression through deacetylating transcription factors such as MyoD and MEF2. HDAC4 is regulated by signaling pathways, and targeting it showed promising results in mitigating muscle wasting [41]. Beclin-1 is a protein involved in the process of autophagy, which is responsible for the degradation and recycling of cellular components in skeletal muscles. Studies have shown that manipulating beclin-1 levels affects muscle mass, with reduced expression attenuating muscle wasting and exacerbating overexpression. However, the precise role of beclin-1 and autophagy in skeletal muscle atrophy is complex and requires further investigation [42]. These mechanisms are crucial for understanding muscle disorder pathogenesis and developing potential therapeutic interventions.

Currently, the management approaches for skeletal muscle atrophy encompass various interventions such as physical exercise, nutritional supplementation, medications, and alternative modalities. Exercise is the most efficacious therapeutic strategy for skeletal muscle atrophy among these but not feasible for all individuals. Regrettably, there is a lack of approved pharmacological treatments and effective remedies for skeletal muscle atrophy available in the market. Consequently, exploring and identifying novel pharmaceutical agents to effectively combat muscle atrophy is imperative. Garlic, which belongs to *Allium* genus, is well known for its abundant natural antioxidants and impressive medicinal properties since ancient times. Garlic exhibits many health benefits, including antibacterial, antifungal, antiviral, anti-inflammatory, and anti-cancer properties. These medicinal properties are attributed to the presence of organosulfur and polyphenol compounds in garlic, making it a valuable resource for medicinal purposes [43-45]. In the current study, we have made an approach to target the skeletal muscle atrophy-associated proteins by utilizing garlic-identified natural compounds through molecular docking. Current study findings will provide some efficient compounds that can be evaluated further *in vitro* or *in vivo* to develop therapeutics for skeletal muscle atrophy.

2. MATERIALS AND METHODS

2.1. Selection and Preparation of Receptors

The crystal structure of HDAC4:2VQM and DNA binding domain of Nuclear factor kappa-light-chain-enhancer of activated B cells (NFkB:1SVC) was retrieved from Protein Data Bank (PDB) (https://www.rcsb.org/) [46,47]. Complete crystal structures for Beclin1, Atrogin, insulin-like growth factor 1 (IGF1), mTOR, Murf1, and Myostatin were unavailable on the PDB; therefore, structures of

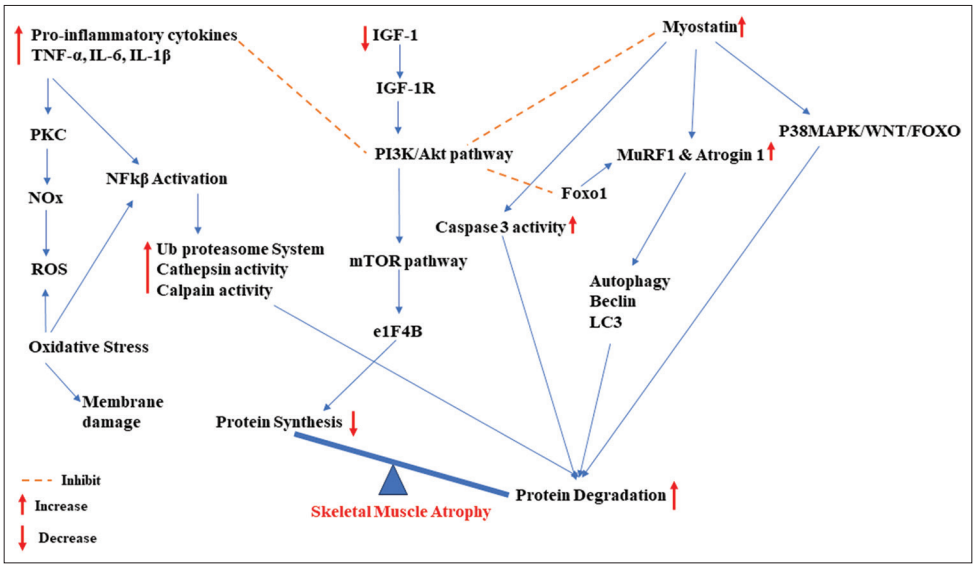

Figure 1: Mechanism of skeletal muscle atrophy.

these proteins were downloaded from the AlphaFold protein structure database. AlphaFold is an AI system developed by Deep Mind for protein structure prediction, which predicts structure with high accuracy and speed [48]. The structure of HDAC4 and NFkB was cleaned by removing non-standard co-crystalized molecules (e.g., water, ligand/s, and phosphates). All the receptors were prepared for docking using the DockPrep tool of chimera-1.16 with default parameters [49].

2.2. Selection of Ligands

We prepared different garlic extracts (fresh, dry, heated, and aged) with 50% methanol, n-butanol, and ethyl acetate (Only fresh garlic). Then, these extracts were subjected to HR-LCMS-QTOF analysis (IIT Bombay, India). We detected approximately 375 compounds (Supplementary File 1), and all these compounds were used as ligands to target different skeletal muscle atrophy-associated proteins.

2.3. Screening of Ligands

Pharmacokinetic (pk) properties for the ligands were predicted using pkCSM (a machine learning-based platform to predict pk of small molecules) [50]. SMILES of each compound were obtained from PubChem (https://pubchem.ncbi.nlm.nih.gov/) [51] and used as input on pkCSM (https://biosig.lab.uq.edu.au/pkcsm/). Selected predicted pk values were used for screening to obtain compounds with desired absorption, distribution, metabolism, excretion, and toxicity (ADMET) profiles. All the compounds were first screened on the basis of Caco-2 permeability (used for prediction of absorption of orally administered drug), and all the compounds with log (Papp) values more than 0.90 were selected. Compounds obtained after the first screening were analyzed for predicted human intestinal absorption values >30%. As compounds with the potential to cross blood-brain barrier (BBB) may cause side effects or toxicity in the brain, predicted BBB permeability values were used to select compounds with logBB<−1. At last, compounds were also analyzed to determine whether they have the potential to cause AMES toxicity or inhibit hERG I/II. Only those compounds that were negative as hERG I/II inhibitors and AMES toxicity were selected and their 3D structure were downloaded from PubChem for further studies.

2.4. Docking Studies

AutoDockTool-1.5.6 [52] module of MGLTools-1.5.6 was used for preparing the grid parameter file (.gpf) and docking parameter file (.dpf) for each receptor and ligand pair. Receptors were blindly docked with selected standards to find their most probable binding site over a receptor. For this, receptors were imported in AutoDockTool-1.5.6, and Kollman charges were added followed by the computation of Gasteiger charges. Ligand was added after protein, and its rotatable bonds were detected automatically and selected as torsion. Ligands were saved in pdbqt (PDB file with added information of charges and torsions) format. For blind docking, whole protein was provided in the grid box for docking. The parameter of grid boxes for Atrogin (grid size: [266, 208, 216], Grid center: [13.984, −11.025, −5.156], spacing 0.375 Å), Myostatin (grid size: [222, 148, 230], grid center: [−1.904, 6.611, 2.852], spacing: 0.375 Å), NFkB ([188, 174, 152], [41.605, 13.011, 42.243], 0.4 Å), Murf1 (grid size: [390, 156, 356], grid center: [−13.156, 5.191, −8.269], spacing 0.4 Å), mTOR ([grid size: 324, 338, 332], grid center: [−1.5, 11.599, −8.661], spacing 0.45 Å), HDAC4 ([grid size: 172 214 126], grid center: [21.337 85.419 25.307], spacing 0.375 Å). Beclin1 was docked with selected ligands directly as no standard drug was available for Beclin1 and IGF1 was docked with Gherlin28 (protein) as standard using Hex 8.0.0 [53]. In case of IGF1 docking with Gherlin28 in hex shape, electro was selected as the correlation type while lest of the parameters were unchanged. The maximum cluster site on the receptors were considered as a potential binding site for their corresponding standard and the same were used for specific docking against the selected ligands, a grid box of (140, 134, 146), (120, 166, 92), (122, 220, 144), (150, 150, 150), (102, 86, 100), (240, 270, 394) with grid center at (3.984, −16.025 2.844), (17.337, 79.419, 34.307), (13.33, −16.901, 3.888), (13.5, 6.599, −22.661), (35.464, 17.682, 35.039), (0.096, −0.389, −23.148) and spacing of 0.375 Å for Atrogin, HDAC4, IGF1, mTOR, NFkB, and Myostatin respectively. Grid box of (394, 156, 402), (390, 156, 356) with grid center at (23.669, 13.829, −48.662), (−13.156, 5.191, −8.269) and spacing of 0.45 Å, 0.4 Å for Beclin, Murf1, respectively. A genetic algorithm was used with 100 runs, 300 population size, and the rest of the parameters were kept default as search parameters.

2.5. Interactions Study

Interactions between protein-protein and protein-ligand were studied using the LigPlus tool [54]. To study interactions of protein-protein complex, protein-ligand (for each pair of ligand and receptor) complexes were generated using Hex 8.0.0 and AutoDockTool-1.5.7, respectively. Interacting residues and H-bonding between receptor and ligands were noted and compared with standard.

3. RESULTS AND DISCUSSIONS

3.1. Screening Analysis

A set of 375 compounds were primarily screened based on ADME/T properties. Absorption property of molecules was predicted for Caco-2 permeability and intestinal absorption; 245 molecules were screened out on the basis of predicted Caco-2 permeability. The remaining 130 molecules were studied for their potential to cross the BBB and only five molecules were selected on the basis of predicted BBB permeability. These 5 molecules were negative for AMES, hERG, and Hepatotoxicity. These 5 compounds (Acetyl tributyl citrate, Adenine, Austalide A, Austalide C, Citromitin) were used as ligands to study their interactions with selected skeletal muscle receptors. Docking results are compiled in Table 1 which shows interactions of ligands and receptors showing their interacting residues and bonding and Table 2 represents the binding energies of ligands after docking with targeted receptors.

3.2. Docking Analysis

HDAC4 docking with selected molecules shows that only Austalide A (−7.32 kcal/mol) can bind with HDAC4 better than Trichostatin A (−6.96 kcal/mol) in the same pocket and interacting with similar residues with the receptor as Trichostatin. In literature, apigenin, luteolin, dihydropyrimidines, dihydroxycinnamic acids, andrographidine showed a binding affinity with different HDAC isoforms with different binding energies [55-58].

Eicosapentaenoic acid binds NFkB with −5.81 kcal/mol whereas among selected natural compounds Austalide A, Austalide C, Citromitin were binding tightly to NFkB with B. E. −7.36 kcal/mol, −6.51 kcal/mol, −6.31 kcal/mol, respectively which is greater than the standard and Citromitin is interacting with almost similar residues as standard.

Adenine (−4.99 kcal/mol) is binding with comparable energy while Austalide A (−6.85 kcal/mol), Austalide C (−7.37 kcal/mol) and

Table 1: Interactions of ligands and receptors showing their interacting residues and bonding.

Receptors (With BE of Standard)→/ Ligands↓	HDAC4	NFkB (-5.81 kcal/mol)	Atrogin (-4.15 kcal/mol)	Murf1 (-3.75 kcal/ mol)	mTOR (-6.60 kcal/mol)	Myostatin (-4.53 kal/mol)	IGF1 (-78.58 kcal/mol)	Beclin (No Standard)
Standards	**HydPho**: His332, Arg37, His158, **Phe227**, **Phe168**, **Gly167**, His159, Pro156, Asp290, Gly330 **H-B**: Gly331, His198, ZN1415	**HydPho**: Met166, Thr163, Val108, Leu160, Phe109, Lys105, Lys106 **H-B**: Lys164	**HydPho**: Gly12, Phe3, Pro2, Leu4, Asn14 **H-B**: Gln13, Trp15	**HydPho**: Cys44, Cys26, Thr31, Cys47 **H-B**: Lys46, Glu28	**HydPho**: Gln2223, Pro2241, Ser913, Ala914, Val915, Gly2238, Phe2184, Phe2182, Trp2239, Val2240 **H-B**: Ser916, Val2183, Glu2881	**HydPho**: Leu270, Arg283, Gly269, Asp370, Phe268, Arg266, Glu107, Arg371, Asp267 **H-B**: Asp271	**HydPho**: Ser45, Thr41, Ala56, Asp60, Gln63, Phe64, Cys38, Phe42 SB: His8 (Lig)---Glu57 (Rec)	NA
Acetyl tributyl citrate	Not considered	Not considered	Not considered	Not considered	Not considered	Not considered	Not considered	Not considered
Adenine	Not considered	Not considered	**HydPho**: Leu180, Val188, Leu186, Ile193, Ser187 **H-B**: Leu189, Val184	**HydPho**: Phe30, Pro24 **H-B**: Asn42, Gln20, Lys19, Ile22	Not considered	**HydPho**: Trp215, Lys141, Leu216 **H-B**: Asn222, Phe142	Not considered	Not considered
Austalide A	**HydPho**: **Phe227**, Met166, Pro165, Tyr79, Glu120, Cys169 **H-B**: **Gly167**, **Phe168**, Tyr170	**HydPho**: Arg15 His25, Gly26, Pro29, Lys38, Gly27, Gly13, Phe14 **H-B**: Arg17	**HydPho**: Gly5, Gln13, Trp15, Pro2, Trp22, Met1, Phe3	**HydPho**: Arg79, Gln185, Asp182, Ala55, Arg72, Phe73, Ile25, Ile51, Pro76, Cys75 **H-B**: Arg74	**HydPho**: Gly2203, Ser909, Asp911, Asp912, Gln2223, Ser913, Asp907, Ala2210, Gln908, Arg2224, Thr2207 **H-B**: Asn2206, Arg910	**HydPho**: Asp99, Ser101, Asp100, Arg98, Lys305, Ile348, Tyr304, Tyr94, Val368, Pro347, Gln97, Asn307 **H-B**: Asn349	**HydPho**: Val65, Asp101, Cys100, Leu102, Leu105, Phe64, Cys38, Ala61, Asp60, Phe42, Leu53, Glu57	**HydPho**: Phe447, Lys450, Ser444, Lys265, Tyr448, Asn268, Thr267, Phe270, Val269, Lys320, Leu264
Austalide C	Not considered	**HydPho**: Asn208, Gly13, Phe14, Gly26, His25, Gly27, Pro29, Leu28, Tyr40 **H-B**: Lys38, Lys10	**HydPho**: Gly12, Trp15, Trp22, Pro2, Met1, Phe3, Gly5 **H-B**: Gln13	**HydPho**: Tyr249, Lys297, Gly296, Thr298, Leu245, Ile242, Ile246 **H-B**: Gln250	**HydPho**: Ser922, Gly2179, His2180, Val915, Phe2182, Trp2239, Pro2241, Leu917, Ser920 **H-B**: Glu2181	**HydPho**: Val368, Tyr94, Pro301, Gln97, Ile348, Asp100, Ser101, Ser346, Pro347 **H-B**: Lys363, Asn349	**HydPho**: Phe42, Leu39, Phe64, Leu102, Leu105 **H-B**: Cys100	**HydPho**: Lys265, Tyr448, Lys450, Phe447, Ser444, Thr267, Val267, Leu264 **H-B**: Asn268
Citromitin	Not considered	**HydPho**: Met166, Glu165, Val108, Thr163, Lys107, Lys106, Lys105 **H-B**: Lys164	**HydPho**: Pro11, Gly5, Trp22, Pro2, Phe3, Leu4, Gly12 **H-B**: Gln13, Trp15	**HydPho**: Gln250, Ile246, Leu245, Thr298, Lys297, Tyr249, Leu253	**HydPho**: His2242, Trp2239, Gly2238, Val2183, Phe2184, Phe2182, Ala914, Ser913, Tyr2225, Val915, Val2240, Arg2224, Pro2241, Ser916, Leu917 **H-B**: Ala2226	**HydPho**: Asn40, Arg333, Gly337, Asn331, Cys339, Glu312, Cys313, Ala41, Trp44	**HydPho**: Ser99, Leu102, Ala61, Phe64, Leu105, Phe42, Cys95, Leu53, Leu58 **H-B**: Cys100	**HydPho**: Gln326, Arg329, Tyr328, Phe325, Ala318, Asn319, His315, Gly322, Lys324, Leu323, Leu324 **H-B**: Leu330

Similarity in interacting residues (Between standard and ligands) Similarity in interacting residues (within selected ligands) Unique interactions, **HydPho**: Hydrophobic, **H-B**: Hydrogen-Bonding.

Table 2: Binding energies of ligands after docking with targeted receptors.

Receptors (With BE of Std.)→/ Ligands↓	HDAC4 (-6.96 kcal/mol)	NFkB (-5.81 kcal/mol)	Atrogin (-4.15 kcal/mol)	Murf1 (-3.75 kcal/mol)	mTOR (-6.60 kcal/mol)	Myostatin (-4.53 kal/mol)	IGF1 (-78.58 kcal/mol)	Beclin (No Standard)
Acetyl tributyl citrate	−3.52	−3.21	−3.31	−2.71	−3.07	−3.49	−2.74	−3.82
Adenine	−4.52	−4.69	−4.99	−4.56	−4.51	−4.56	−4.67	−4.18
Austalide A	−7.32	−7.36	−6.85	−7.05	−7.81	−8.71	−7.81	−7.54
Austalide C	−6.82	−6.51	−7.37	−6.40	−7.82	−8.34	−6.28	−6.88
Citromitin	−5.97	−6.31	−6.69	−5.42	−7.19	−6.66	−6.00	−6.03

All binding energies (B. E.) are in kcal/mol. Ligands: Selected ligands after screening, : Ligands with Binding affinity >Corresponding standards, : Ligands with Binding affinity non-comparable due to different docking algorithm used for standard (peptide) undergoing Protein Protein docking. : Ligands with good Binding affinity without any Corresponding standards, HDAC: Histone deacetylase, NFkB: Nuclear factor kappa B, mTOR: Mammalian target of the rapamycin, IGF1: Insulin like growth factor 1.

Citromitin (−6.69 kcal/mol) are binding strongly with atrogin as compared to meloxicam (−4.15 kcal/mol). Interacting residues of atrogin with meloxicam were similar in austalide A and austalide C. Interacting residues of citromitin showed maximum similarity with the set of residues interacting with standard.

Murf1 is binding to meloxicam with B. E. −3.75 kcal/mol only, whereas 4 out of 5 selected compounds show tight binding with target receptor. When their interacting residues were compared with the standard, no similarity was found. However, adenine and austalide A were binding around the same pocket except for austalide C and citromitin.

Docking studies on mTOR wee performed to find a better candidate than resveratrol (−6.60 kcal/mol) to activate mTOR, and after analyzing the docking results of the selected compounds, it was found that austalide A, austalide C, and citromitin can be good candidates to replace the standard (resveratrol) because they are binding energy with −7.81 kcal/mol, −7.82 kcal/mol, and −7.19 kcal/mol. When interacting residues were compared, maximum residues were common in austalide C, citromitin, and resveratrol.

Myostatin binds formoterol with B. E. −4.53 kcal/mol, similar to the B. E. of adenine (−4.56 kcal/mol) but has much lower B. E. than austalide A (−8.71 kcal/mol), austalide C (−8.34 kcal/mol), and citromitin (−6.66 kcal/mol). This makes them a good drug candidate to inhibit myostatin. No common interacting residues were found when ligands were compared with the standard. Dithymoquinone inhibited myostatin with a binding free energy of −7.40 kcal/mol, which is lower than austalide A and austalide C used in our study [59]. Curcumin and gingerol also showed specific binding with myostatin among 38,000 Chinese traditional compounds with higher binding affinity than our tested compounds [60]. Catechin and epicatechin exhibited stronger bond with myostatin with energy −6.90 kcal/mol and −7.0 kcal/mol respectively which is lower than austalide A and C [61].

In case of IGF1 protein-protein docking was performed as its activator (Ghrelin 28) is a peptide. Ghrelin 28, being a peptide, binds to IGF1 with −78.58 kcal/mol, which is higher than the non-peptide drug candidates austalide A (−7.81 kcal/mol), austalide C (−6.28 kcal/mol), and citromitin (−6.00 kcal/mol), these three molecules are binding to the same binding site where ghrelin 28 binds. Hence, they may be better activator for IGF1 but due to difference between the nature of standard and selected ligands it is difficult to interpret whether selected candidates can replace Ghrelin 28 as a better activator or not. We found that Austalide A, Austalide C, and Citromitin bind at the same site as Ghrelin 28 and interact with similar residues. In literature, catechins found in black tea showed significant binding with IGF1 with higher binding energy than reported in our study [62]. Apigenin and luteolin binds to IGF1 with −5.78 kcal.mol and −5.70 kcal/mol respectively, which is lower than austalide A, C and Citromitin [63]. Therefore, further docking studies and molecular dynamic simulation is required to confirm their potential as a good activator.

Beclin1 was docked blindly as no standard was not available for this target but based on binding energies of selected ligands austalide A, austalide C, and citromitin with B. E. −7.81 kcal/mol, −6.28 kcal/mol, and −6.00 kcal/mol respectively can be potential inhibitors of Beclin1 but a comparative docking study of Beclin1 with its inhibitor is further required. Interaction analysis showed that top three standards were binding in similar pockets.

After analyzing all the docking results, it is clear that austalide A can be a potential lead molecule as it is showing better binding with almost all the targets if compared with other molecules [Figure 2]. Austalide A is a polyketide compound classified as a natural product, isolated from the marine fungus *Aspergillus ustus*. Notably, Austalide A possesses a distinct chemical structure characterized by a macrolactone ring that is highly oxygenated [64]. This compound has attracted considerable scientific interest due to its exceptional biological activities, including its anticancer, antiviral, and anti-osteoporosis properties [65]. Recently, a computational study (*in silico*) investigated austalide X and demonstrated its potential in cancer prevention and the inhibition of COVID-19 infection. The study revealed promising pk and pharmacodynamic characteristics of austalide X [66]. In addition, austalides V and W exhibited significant anticancer effects against prostate and bladder cancer cells [67]. Moreover, austalide K demonstrated an anti-osteoporosis effect by inhibiting the differentiation of osteoclasts induced by the receptor activator of nuclear factor-κB ligand (RANKL) and enhancing the differentiation of osteoblasts mediated by bone morphogenetic protein-2, without causing harm to cells [68].

Despite the limited literature on austalides, it offers a broad scope for exploring the therapeutic potential of these compounds in various medical conditions. While austalide A has not been specifically investigated through *in silico* studies, the existing literature strongly indicates that austalides exhibit substantial anticancer activity and possess diverse biological properties that can be harnessed to treat different medical conditions. Notably, our own study demonstrated the ability of austalide A to bind to all targets associated with

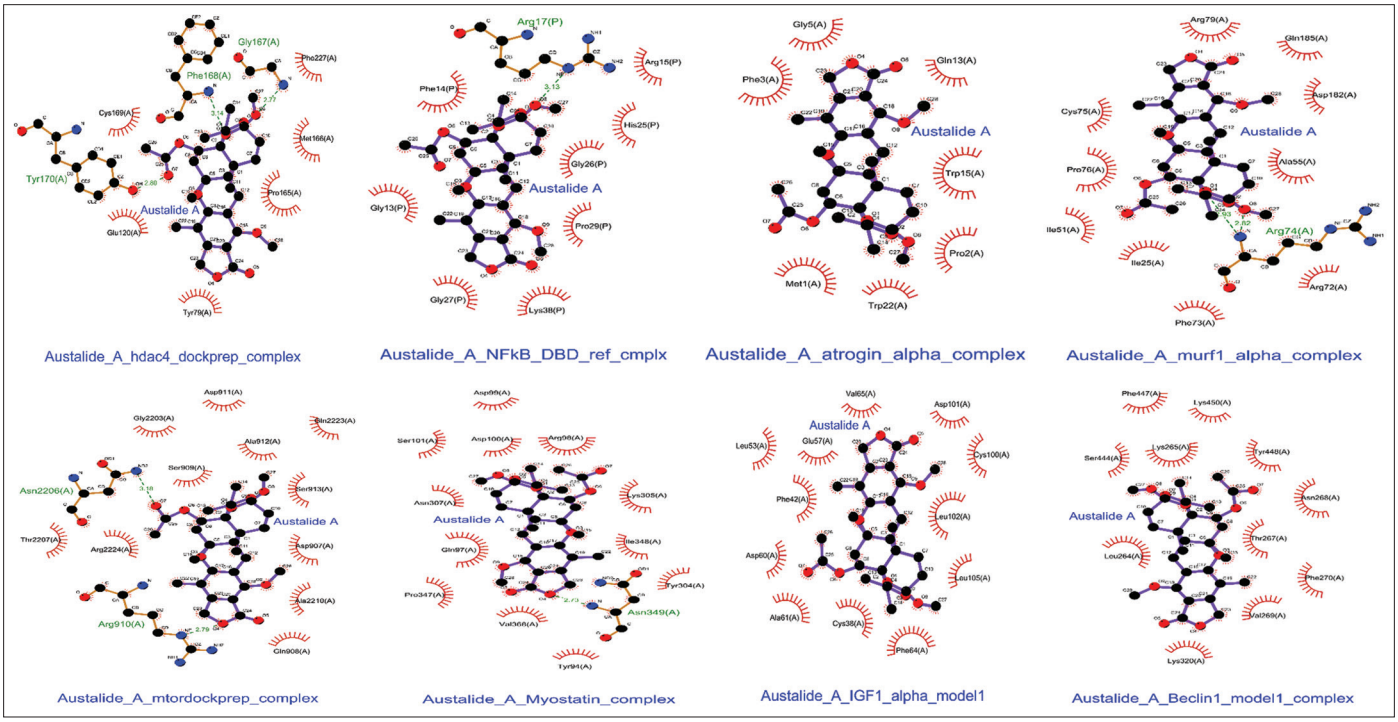

Figure 2: Molecular docking of complex austalide A with selected skeletal muscle atrophy targets.

skeletal muscle atrophy, providing a promising avenue for further investigations into its therapeutic properties in preventing skeletal muscle atrophy.

4. CONCLUSION

The utilization of docking studies is essential for researchers to comprehensively understand how ligands interact with therapeutic targets, playing a crucial role in structure-based drug discovery by identifying new biologically active compounds. The present study conducted molecular docking investigations, focusing on proteins related to skeletal muscle atrophy and the natural compounds found in garlic. This research revealed that the tested garlic compounds effectively bind to skeletal muscle atrophy-associated targets. Austalide A, a prominent component, exhibits particularly strong affinity due to intermolecular hydrogen bonding and hydrophobic interactions, albeit with varying binding energies for different receptors. However, it is necessary to emphasize the need for further research into the intricate molecular pathways of these compounds before considering their potential as treatments for skeletal muscle atrophy.

5. ACKNOWLEDGEMENTS

The scholarly research work was fully validated by The Council of Scientific & Industrial Research (CSIR) fellowship, Delhi, India. Researchers are grateful to SAIF, IIT Bombay, Mumbai, for HR-LCMS-QTOF data.

6. AUTHORS' CONTRIBUTIONS

All authors made substantial contributions to the conception and design, acquisition of data, or analysis and interpretation of data; took part in drafting the article or revising it critically for important intellectual content; agreed to submit to the current journal; gave final approval of the version to be published; and agreed to be accountable for all aspects of the work. All the authors are eligible to be an author as per the International Committee of Medical Journal Editors (ICMJE) requirements/guidelines.

7. FUNDING

This study was fully funded by the Council of Scientific & Industrial Research (CSIR) fellowship, Delhi, India.

8. CONFLICTS OF INTEREST

The authors report no financial or any other conflicts of interest in this work.

9. ETHICAL APPROVALS

This study does not involve experiments on animals or human subjects.

10. DATA AVAILABILITY

All the data is available with the authors and shall be provided upon request.

11. PUBLISHER'S NOTE

This journal remains neutral with regard to jurisdictional claims in published institutional affiliation.

REFERENCES

1. Frontera WR, Ochala J. Skeletal muscle: A brief review of structure and function. Calcif Tissue Int 2015;96:183-95.
2. Henderson CA, Gomez CG, Novak SM, Mi-Mi L, Gregorio CC. Overview of the muscle cytoskeleton. Compr Physiol 2017;7:891-944.
3. Gelfi C, Vasso M, Cerretelli P. Diversity of human skeletal muscle

in health and disease: Contribution of proteomics. J Proteomics 2011;74:774-95.
4. Dutt V, Gupta S, Dabur R, Injeti E, Mittal A. Skeletal muscle atrophy: Potential therapeutic agents and their mechanisms of action. Pharmacol Res 2015;99:86-100.
5. Yin L, Li N, Jia W, Wang N, Liang M, Yang X, *et al.* Skeletal muscle atrophy: From mechanisms to treatments. Pharmacol Res 2021;172:105807.
6. Chemello F, Bean C, Cancellara P, Laveder P, Reggiani C, Lanfranchi G. Microgenomic analysis in skeletal muscle: Expression signatures of individual fast and slow myofibers. PLoS One 2011;6:e16807.
7. Shen Y, Zhang Q, Huang Z, Zhu J, Qiu J, Ma W, *et al.* Isoquercitrin delays denervated soleus muscle atrophy by inhibiting oxidative stress and inflammation. Front Physiol 2020;11:988.
8. Park J, Cho J, Song EJ. Ubiquitin-proteasome system (UPS) as a target for anticancer treatment. Arch Pharm Res 2020;43:1144-61.
9. Lee JH, Jeon JH, Lee MJ. Docosahexaenoic acid, a potential treatment for sarcopenia, modulates the ubiquitin-proteasome and the autophagy-lysosome systems. Nutrients 2020;12:2597.
10. Sorimachi H, Imajoh-Ohmi S, Emori Y, Kawasaki H, Ohno S, Minami Y, *et al.* Molecular cloning of a novel mammalian calcium-dependent protease distinct from both m- and mu-types. Specific expression of the mRNA in skeletal muscle. J Biol Chem 1989;264:20106-11.
11. Tipton KD, Hamilton DL, Gallagher IJ. Assessing the role of muscle protein breakdown in response to nutrition and exercise in humans. Sports Med 2018;48:53-64.
12. Ito N, Ruegg UT, Takeda S. ATP-induced increase in intracellular calcium levels and subsequent activation of mTOR as regulators of skeletal muscle hypertrophy. Int J Mol Sci 2018;19:2804.
13. Powers SK. Can antioxidants protect against disuse muscle atrophy? Sports Med 2014;44 Suppl 2:S155-65.
14. Silva KA, Dong J, Dong Y, Dong Y, Schor N, Tweardy DJ, *et al.* Inhibition of Stat3 activation suppresses caspase-3 and the ubiquitin-proteasome system, leading to preservation of muscle mass in cancer cachexia. J Biol Chem 2015;290:11177-87.
15. Webster JM, Kempen LJ, Hardy RS, Langen RC. Inflammation and skeletal muscle wasting during cachexia. Front Physiol 2020;11:597675.
16. Zhou J, Liu B, Liang C, Li Y, Song YH. Cytokine signaling in skeletal muscle wasting. Trends Endocrinol Metab 2016;27:335-47.
17. Baehr LM, West DW, Marshall AG, Marcotte GR, Baar K, Bodine SC. Muscle-specific and age-related changes in protein synthesis and protein degradation in response to hindlimb unloading in rats. J Appl Physiol (1985) 2017;122:1336-50.
18. Banerjee R, He J, Spaniel C, Quintana MT, Wang Z, Bain J, *et al.* Non-targeted metabolomics analysis of cardiac muscle ring finger-1 (MuRF1), MuRF2, and MuRF3 *in vivo* reveals novel and redundant metabolic changes. Metabolomics 2015;11:312-22.
19. Boutari C, Mantzoros CS. Decreasing lean body mass with age: Challenges and opportunities for novel therapies. Endocrinol Metab (Seoul) 2017;32:422-5.
20. Mulder E, Clément G, Linnarsson D, Paloski WH, Wuyts FP, Zange J, *et al.* Musculoskeletal effects of 5 days of bed rest with and without locomotion replacement training. Eur J Appl Physiol 2015;115:727-38.
21. Peris-Moreno D, Cussonneau L, Combaret L, Polge C, Taillandier D. Ubiquitin ligases at the heart of skeletal muscle atrophy control. Molecules 2021;26:407.
22. McGrath MJ, Eramo MJ, Gurung R, Sriratana A, Gehrig SM, Lynch GS, *et al.* Defective lysosome reformation during autophagy causes skeletal muscle disease. J Clin Invest 2021;131:135124.
23. Moresi V, Williams AH, Meadows E, Flynn JM, Potthoff MJ, McAnally J, *et al.* Myogenin and class II HDACs control neurogenic muscle atrophy by inducing E3 ubiquitin ligases. Cell 2010;143:35-45.
24. Moresi V, Carrer M, Grueter CE, Rifki OF, Shelton JM, Richardson JA, *et al.* Histone deacetylases 1 and 2 regulate autophagy flux and skeletal muscle homeostasis in mice. Proc Natl Acad Sci U S A 2012;109:1649-54.
25. Raben N, Hill V, Shea L, Takikita S, Baum R, Mizushima N, *et al.* Suppression of autophagy in skeletal muscle uncovers the accumulation of ubiquitinated proteins and their potential role in muscle damage in Pompe disease. Hum Mol Genet 2008;17:3897-908.
26. Rocchi A, He C. Regulation of exercise-induced autophagy in skeletal muscle. Curr Pathobiol Rep 2017;5:177-86.
27. Connolly P, Garcia-Carpio I, Villunger A. Cell-cycle cross talk with caspases and their substrates. Cold Spring Harb Perspect Biol 2020;12:a036475.
28. Nelson WB, Smuder AJ, Hudson MB, Talbert EE, Powers SK. Cross-talk between the calpain and caspase-3 proteolytic systems in the diaphragm during prolonged mechanical ventilation. Crit Care Med 2012;40:1857-63.
29. Ottenheijm CA, Heunks LM, Li YP, Jin B, Minnaard R, van Hees HW, *et al.* Activation of the ubiquitin-proteasome pathway in the diaphragm in chronic obstructive pulmonary disease. Am J Respir Crit Care Med 2006;174:997-1002.
30. Wang XH, Mitch WE. Mechanisms of muscle wasting in chronic kidney disease. Nat Rev Nephrol 2014;10:504-16.
31. Aweida D, Rudesky I, Volodin A, Shimko E, Cohen S. GSK3-β promotes calpain-1-mediated desmin filament depolymerization and myofibril loss in atrophy. J Cell Biol 2018;217:3698-714.
32. Dókus LE, Yousef M, Bánóczi Z. Modulators of calpain activity: Inhibitors and activators as potential drugs. Expert Opin Drug Discov 2020;15:471-86.
33. Kramerova I, Torres JA, Eskin A, Nelson SF, Spencer MJ. Calpain 3 and CaMKIIβ signaling are required to induce HSP70 necessary for adaptive muscle growth after atrophy. Hum Mol Genet 2018;27:1642-53.
34. Munkanatta Godage DN, VanHecke GC, Samarasinghe KT, Feng HZ, Hiske M, Holcomb J, *et al.* SMYD2 glutathionylation contributes to degradation of sarcomeric proteins. Nat Commun 2018;9:4341.
35. Ono Y, Saido TC, Sorimachi H. Calpain research for drug discovery: Challenges and potential. Nat Rev Drug Discov 2016;15:854-76.
36. Feldman ME, Apsel B, Uotila A, Loewith R, Knight ZA, Ruggero D, *et al.* Active-site inhibitors of mTOR target rapamycin-resistant outputs of mTORC1 and mTORC2. PLoS Biol 2009;7:e38.
37. Liu GY, Sabatini DM. mTOR at the nexus of nutrition, growth, ageing and disease. Nat Rev Mol Cell Biol 2020;21:183-203.
38. Rindom E, Kristensen AM, Overgaard K, Vissing K, de Paoli FV. Estimation of p70S6K Thr. and 4E-BP1 Thr(37/46) phosphorylation support dependency of tension per se in a dose-response relationship for downstream mTORC1 signaling. Acta Physiol (Oxf) 2020;229:e13426.
39. Winbanks CE, Weeks KL, Thomson RE, Sepulveda PV, Beyer C, Qian H, *et al.* Follistatin-mediated skeletal muscle hypertrophy is regulated by Smad3 and mTOR independently of myostatin. J Cell Biol 2012;197:997-1008.
40. Zhou Y, Hellberg M, Hellmark T, Höglund P, Clyne N. Muscle mass and plasma myostatin after exercise training: A substudy of renal exercise (RENEXC)-a randomized controlled trial. Nephrol Dial Transplant 2021;36:95-103.
41. Mielcarek M, Toczek M, Smeets CJ, Franklin SA, Bondulich MK, Jolinon N, *et al.* HDAC4-myogenin axis as an important marker of HD-related skeletal muscle atrophy. PLoS Genet 2015;11:e1005021.
42. Singh A, Phogat J, Yadav A, Dabur R. The dependency of autophagy and ubiquitin proteasome system during skeletal muscle atrophy. Biophys Rev 2021;13:203-19.
43. Deresse D. Antibacterial effect of garlic (*Allium sativum*) on *Staphylococcu aureus*: An *in vitro* study. Asian J Med Sci 2010;2:62.
44. Mansell TJ. A review of garlic and other alliums: The Lore and the science. Food Foodways 2010;18:170-2.

45. Thomson M, Ali M. Garlic [*Allium sativum*]: A review of its potential use as an anti-cancer agent. Curr Cancer Drug Targets 2003;3:67-81.
46. Bottomley MJ, Lo Surdo P, Di Giovine P, Cirillo A, Scarpelli R, Ferrigno F, *et al.* Structural and functional analysis of the human HDAC4 catalytic domain reveals a regulatory structural zinc-binding domain. J Biol Chem 2008;283:26694-704.
47. Müller CW, Rey FA, Sodeoka M, Verdine GL, Harrison SC. Structure of the NF-kappa B p50 homodimer bound to DNA. Nature 1995;373:311-7.
48. Jumper J, Evans R, Pritzel A, Green T, Figurnov M, Ronneberger O, *et al.* Highly accurate protein structure prediction with AlphaFold. Nature 2021;596:583-9.
49. Pettersen EF, Goddard TD, Huang CC, Couch GS, Greenblatt DM, Meng EC, *et al.* UCSF Chimera-a visualization system for exploratory research and analysis. J Comput Chem 2004;25:1605-12.
50. Pires DE, Blundell TL, Ascher DB. pkCSM: Predicting small-molecule pharmacokinetic and toxicity properties using graph-based signatures. J Med Chem 2015;58:4066-72.
51. Kim S, Chen J, Cheng T, Gindulyte A, He J, He S, *et al.* PubChem 2023 update. Nucleic Acids Res. 2023;51:D1373-80.
52. Sanner MF. Python: A programming language for software integration and development. J Mol Graph Model 1999;17:57-61.
53. Ritchie DW, Kozakov D, Vajda S. Accelerating and focusing protein-protein docking correlations using multi-dimensional rotational FFT generating functions. Bioinformatics 2008;24:1865-73.
54. Laskowski RA, Swindells MB. LigPlot+: Multiple ligand-protein interaction diagrams for drug discovery. J Chem Inf Model 2011;51:2778-86.
55. Ganai SA, Farooq Z, Banday S, Altaf M. *In silico* approaches for investigating the binding propensity of apigenin and luteolin against class I HDAC isoforms. Future Med Chem 2018;10:1925-45.
56. Thipparapu G, Ajumeera R, Venkatesan V. Novel dihydropyrimidine derivatives as potential HDAC inhibitors: *In silico* study. *In silico* Pharmacol 2017;5:10.
57. Anantharaju PG, Reddy DB, Padukudru MA, Chitturi CM, Vimalambike MG, Madhunapantula SV. Induction of colon and cervical cancer cell death by cinnamic acid derivatives is mediated through the inhibition of Histone Deacetylases (HDAC). PLoS One 2017;12:e0186208.
58. Das D, Banerjee R, Bandyopadhyay M, Nag A. Exploring the potential of *Andrographis paniculata* for developing novel HDAC inhibitors: An *in silico* approach. J Biomol Struct Dyn 2023;15:1-13.
59. Ahmad SS, Ahmad K, Lee EJ, Shaikh S, Choi I. Computational identification of dithymoquinone as a potential inhibitor of myostatin and regulator of muscle mass. Molecules 2021;26:5407.
60. Ali S, Ahmad K, Shaikh S, Lim JH, Chun HJ, Ahmad SS, *et al.* Identification and evaluation of traditional Chinese medicine natural compounds as potential myostatin inhibitors: An *in silico* approach. Molecules 2022;27:4303.
61. Sabarathinam S, Rajappan Chandra SK, Satheesh S. Network pharmacology based pharmacokinetic assessment and evaluation of the therapeutic potential of catechin derivatives as a potential myostatin inhibitor: A special view on Sarcopenic Obesity. Nat Prod Res 2023;20:1-5.
62. Firdausi L, Rasjad Indra MR. Binding inhibition between Igf1r and Igf1 by catechin of black tea. J Trop Life Sci 2012;2:132-5.
63. Soni N, Pardasani KR, Mujwar S. *In silico* analysis of dietary agents as anticancer inhibitors of insulin like growth factor 1 receptor (IGF1R). J Pharm Pharm Sci 2015;7:191-6.
64. Horak RM, Steyn PS, Vleggaar R, Rabie CJ. Metabolites of *Aspergillus* ustus. Part 1. Application of the heteronuclear selective population inversion (SPI) nmr technique to the structure elucidation of the austalides A-F, novel ortho ester meroterpenoids. J Chem Soc Perkin Trans 1985;1:345-56.
65. Liu L, Ruan H. An overview of natural austalides: Structure, bioactivity and synthesis. Phytochem Lett 2022;47:81-92.
66. Elnaggar MS, Elissawy AM, Youssef FS, Singab AN. New austalide derivative from the marine-derived *Aspergillus* sp. and evaluation of its biological activity. RSC Adv 2023;13:16480-16487.
67. Antipova TV, Zaitsev KV, Oprunenko YF, Ya Zherebker A, Rystsov GK, Zemskova MY, *et al.* Austalides V and W, new meroterpenoids from the fungus *Aspergillus* ustus and their antitumor activities. Bioorg Med Chem Lett 2019;29:126708.
68. Kim KJ, Lee J, Wang W, Lee Y, Oh E, Park KH, *et al.* Austalide K from the Fungus *Penicillium rudallense* prevents LPS-induced bone loss in mice by inhibiting osteoclast differentiation and promoting osteoblast differentiation. Int J Mol Sci 2021;22:5493.

How to cite this article:
Monika M, Gupta S, Dua A, Mittal A. In silico analysis of garlic phyto-chemicals binding affinities to skeletal muscle atrophy linked factors through molecular docking. JApp Biol Biotech. 2024;12(2):304-311.